AGU Chapman Conference on Particle Dynamics in the Earth's Radiation Belts
Cascais, Portugal, 4-9 March 2018

Roles of upper-hybrid waves on the particle dynamics in the Earth's radiation belt

Junga Hwang[1,2], Peter H. Yoon[1,3,4],
Rodrigo A. López[3], Dae-Kyu Shin[5], William S. Kurth[6], Brian A. Larsen[7,8], Geoff D. Reeves[7,8], Dae-Young Lee[5] and Jaejin Lee[1,2]

[1]Korea Astronomy and Space science Institute, Daejeon 34055, South Korea
[2] Korea University of Science and Technology, Daejeon 34113, South Korea
[3]University of Maryland, College Park, MD 20742, USA
[4]Kyung Hee University, Yongin 17104, South Korea
[5] Chungbuk National University, Cheng-ju 28644, South Korea
[6]University of Iowa, Iowa City, Iowa 52242, USA
[7]ISR-1 Space Science and Applications, Los Alamos National Laboratory, New Mexico 87545, USA
[8]The New Mexico Consortium, New Mexico, New Mexico 87544, USA

Making waves with the hot electrons within Earth's radiation belts

20 June 2017

Credit: CC0 Public Domain

Encircling the Earth, within its magnetosphere, are two concentric, doughnut-shaped radiation belts known as the Van Allen belts. The Van Allen belts swell and recede in response to incoming energy from the sun, sometimes billowing far enough to expose orbiting satellites and other spacecraft to damaging radiation that can disrupt electronic communications and navigation signals, as well as electric grids. These radiation belt electrons travel near the speed of light and emit and absorb waves that are used by scientists to understand space weather.

An international team of scientists recently discovered the role that hot electrons may play in the waves and fluctuations detected by satellites. The research team reports its findings this week in *Physics of Plasmas*. Their results are based on data collected by the Van Allen Probes, twin robotic spacecraft launched by NASA in 2012 to help scientists better understand these belt regions.

Previous research has focused on low-frequency electromagnetic waves emitted from cold electrons as the major cause of acceleration and loss of relativistic electrons. These wave-particle interactions directly affect the width of the bands. Low-frequency waves include whistler-mode plasma waves, so named for the hissing or static sound they make that is audible through a speaker.

This general theory describes electrons from solar wind interacting with these low-frequency plasma waves. This causes the electrons to gain a tremendous amount of energy from the amplification of the whistler-mode waves via the surrounding plasmasphere.

However, according to the research team, low-frequency waves are typically associated with active magnetospheric conditions, which don't always occur. In contrast, high-frequency quasi-electrostatic (ES) fluctuations in the upper-hybrid frequency are a constant and pervasive feature in the Earth's radiation belt environment, as was recently discovered through new data from the Van Allen Probes.

"Occasional low-frequency waves with extremely large amplitudes may suddenly accelerate the electrons," said Junga Hwang, principal researcher at the Korea Astronomy and Space Science Institute in South Korea and a co-author of the paper. "But we believe that it is the high-frequency ES fluctuations that are constantly emitted and reabsorbed by the hot electrons, which allow these radiation belt electrons to remain inside the outer Van Allen band for a long time."

In their study, the researchers looked at electrons at three energy ranges: cold electrons, hot electrons and relativistic electrons. Cold electrons mainly contribute to the background electron density. Hot electrons are known as the main source for wave making. The relativistic electrons, meanwhile, result from particle acceleration processes, but they don't influence average plasma characteristics. The researchers chose "quiet-time" intervals to study the high-frequency waves when the low-frequency plasma waves were absent.

"Since hot electrons constitute only a small fraction of the total electron number density, the general thought has been that the upper-hybrid fluctuations are useful only as a tool for indirectly measuring the cold electron number density," Hwang said. "However, the data from the Van Allen Probes showed that upper-hybrid ES (electrostatic) fluctuations pervasively and ubiquitously exist in the radiation belts. From there, we proved that the presence of hot electrons and upper-hybrid fluctuations are mutually related phenomenon."

More information: J. Hwang et al, Roles of hot electrons in generating upper-hybrid waves in the earth's radiation belt, *Physics of Plasmas* (2017). DOI: 10.1063/1.4984249

Plasma waves in the magnetosphere

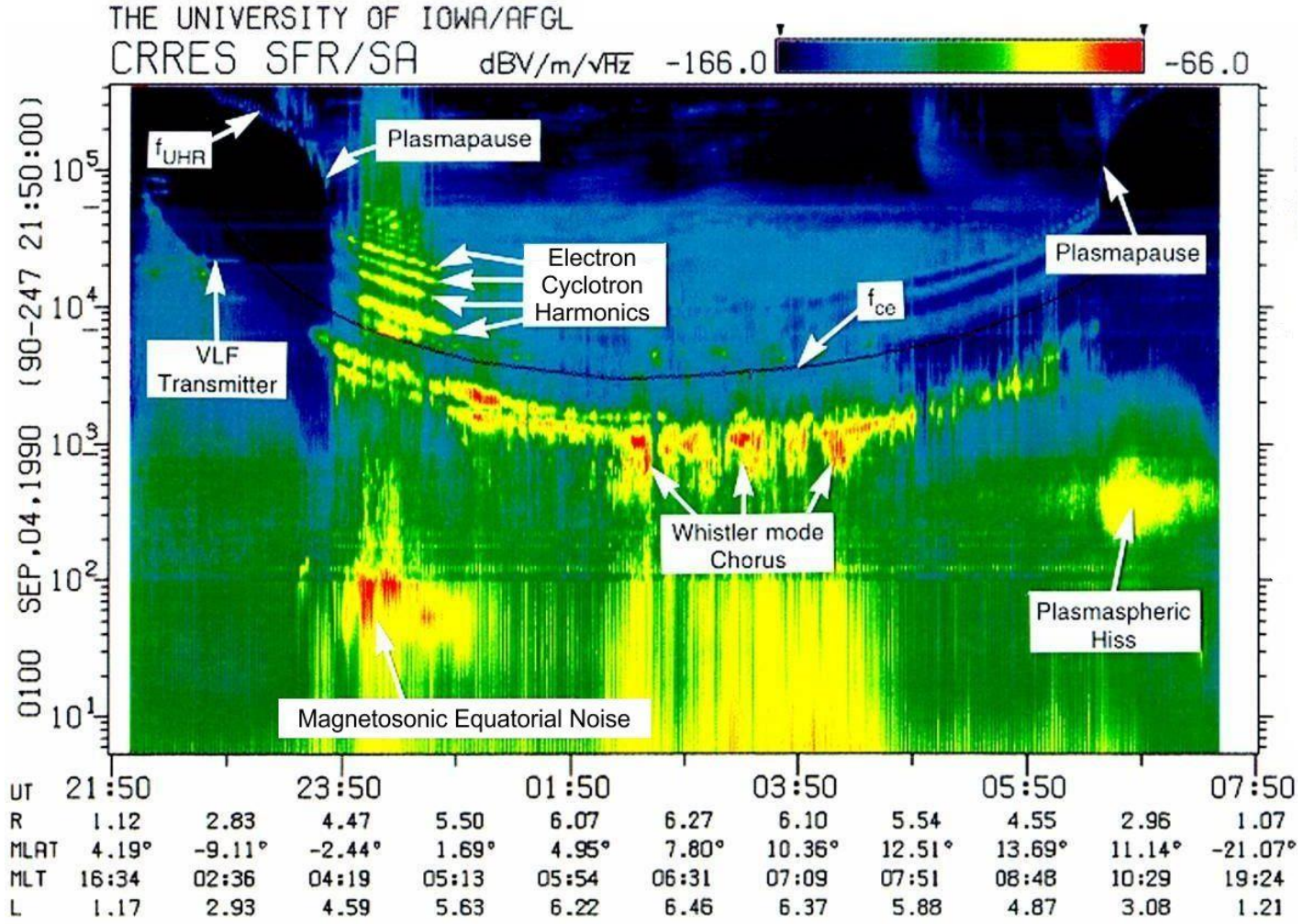

https://emfisis.physics.uiowa.edu/science/introduction

Introduction

- Low-frequency electromagnetic (EM) waves, namely, ultra low frequency waves (ULF), whistler-mode chorus, plasmaspheric hiss, EM ion-cyclotron (EMIC), and magnetosonic (MS) waves known as *equatorial noise* (and sometimes multiple harmonic electron cyclotron waves) receive much attention as efficient acceleration mechanisms for electrons up to relativistic energies in the Earth's radiation belt.

- These low-frequency waves are usually associated with active magnetospheric conditions such that they do not always occur, and when they do, their occurrence is often limited to spatially localized regions.

- In contrast, high-frequency quasi-electrostatic (ES) fluctuations in the upper-hybrid frequency range are a constant and pervasive feature in the Earth's radiation belt environment [*Kurth et al.*, 2015].

- Until now, the ubiquitous upper-hybrid waves utilized only for determining the background electron density.

- The persistent upper-hybrid fluctuations detected by the Waves instrument are analogous to the quasi-thermal noise, or Langmuir fluctuations, in the solar wind [*Meyer-Vernet*, 1979; *Filbert and Kellogg*, 1979; *Meyer-Vernet and Perche*, 1989; *Issautier et al.*, 2001], except that for the radiation belt environment the assumption of weakly-magnetized or unmagnetized plasma must be relaxed.

- For a magnetized plasma, one can have a quasi-thermal emission at the upper hybrid frequency when the plasma is stable and also an instability of upper hybrid waves caused by an unstable electron distribution such as a loss cone or a temperature anisotropy can take place.

- We formulate the theory of ES spontaneous emission in magnetized plasmas, which is applicable for the radiation belt environment. And we expand this work to EM theory, which might be tested by future spacecraft missions.

- Among the first detection of intense upper-hybrid waves in the plasmasphere is by *Kurth et al.* [1979a,1979b], who reported that these emissions are related to unstable electron distributions.

- Some other early works on the magnetospheric upper-hybrid emission and the related $(n + 1/2)fce$ bands include *Hubbard and Birmingham* [1978], *Ashour-Abdalla and Kennel* [1978a, 1978b], *Christiansen et al.* [1978], *Ronnmark et al.* [1978].

- However, all these works are related to **loss cone instability or temperature anisotropy**.

- The present work is similar to these early papers, but the main difference is that we are interested in **quiet-time situations where the electron distribution is quasi-isotropic and no instability mechanism is forthcoming.**

- Of particular interest is the relative contribution of the background, relatively cold, electrons characterized by eV range thermal energy, versus tenuous energetic electrons with tens of keV energy but with typical density, which is of the order of 10^{-4} when compared with that of the background.

Complicated mixture of various electron distributions over various energy ranges in the magnetosphere

- **Cold** electrons: a few eV
- **Hot** electrons: 1-50keV (seed electrons: 10-100keV)
- **Relativistic** electrons: >100keV

- **Question**: What is the relative contribution of cold electrons characterized by the eV range of thermal energy versus hot electrons with tens keV energy but with typical density, which is of the order of 10^{-4} compared to that of the cold electrons to the upper hybrid waves?

- **Data**: electron field measurements by the Waves instrument on Van Allen Probes.
- A primary objective of the higher-frequency measurements is the determination of the electron density n_e at the spacecraft, primarily inferred from the upper hybrid resonance frequency f_{uh}.

$$\omega_{uh}^2 = \omega_{ce}^2 + \omega_{pe}^2$$

Case 1 :
Multiple harmonics UHR, no chorus wave

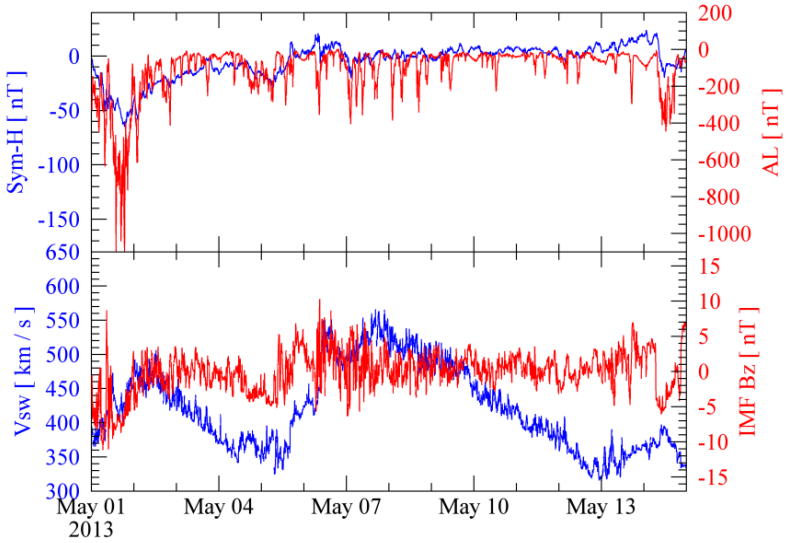

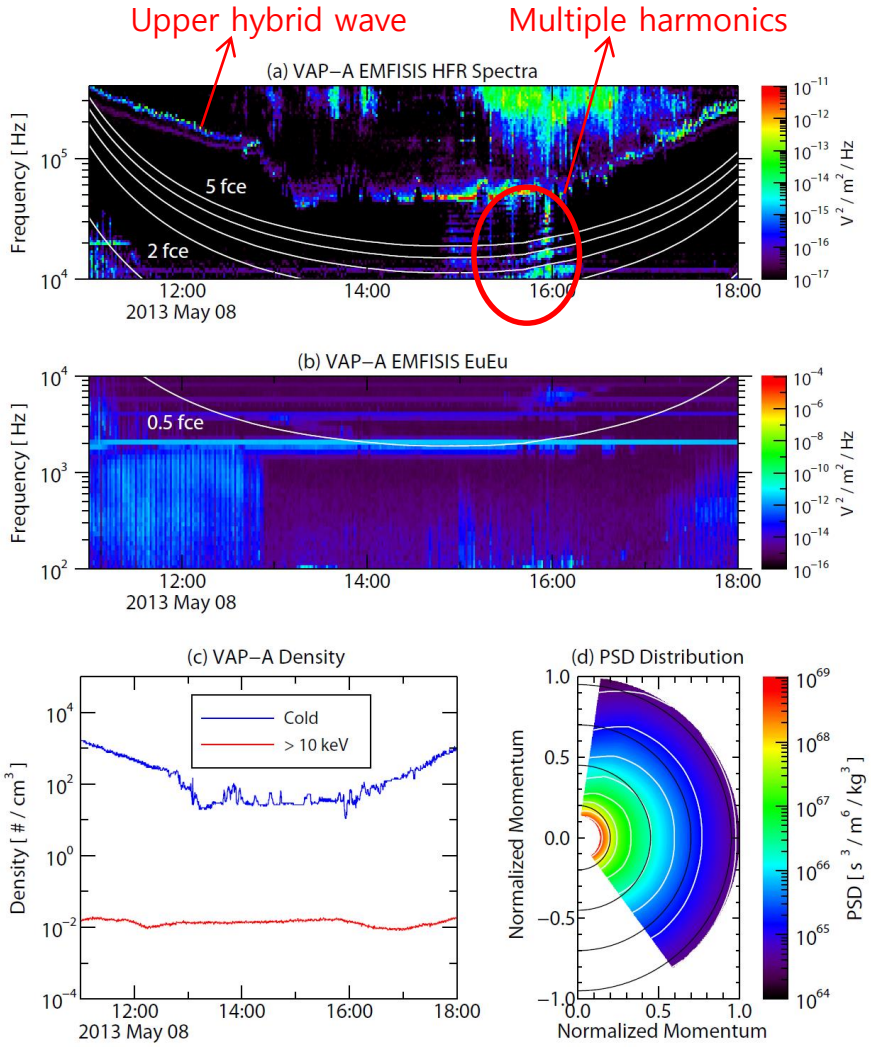

Figure 1. (a) shows the electric field spectrum for May, 8, 2013. Upper-hybrid waves are detected throughout the entire interval of data collection. Multiple-harmonic electron-cyclotron waves below the upper-hybrid frequency are also seen around 16:00. (b), which shows electric field spectrum in the low-frequency band, clearly indicates the absence of whistler-mode chorus waves. (c) plots the cold (blue) and hot (red) electron densities. Panel (d) displays the phase space distribution (PSD).

Hwang et al., 2017

Case 2 :
Single UHR, no chorus wave

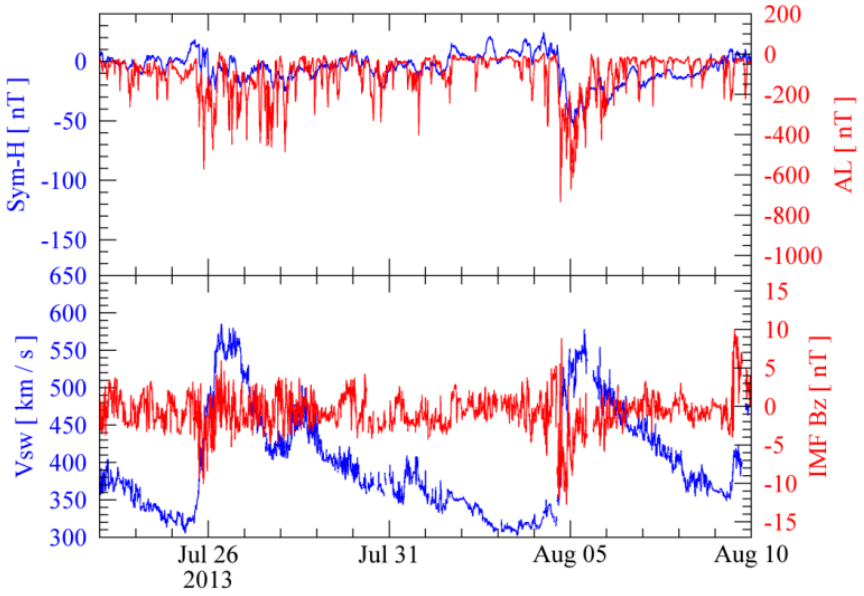

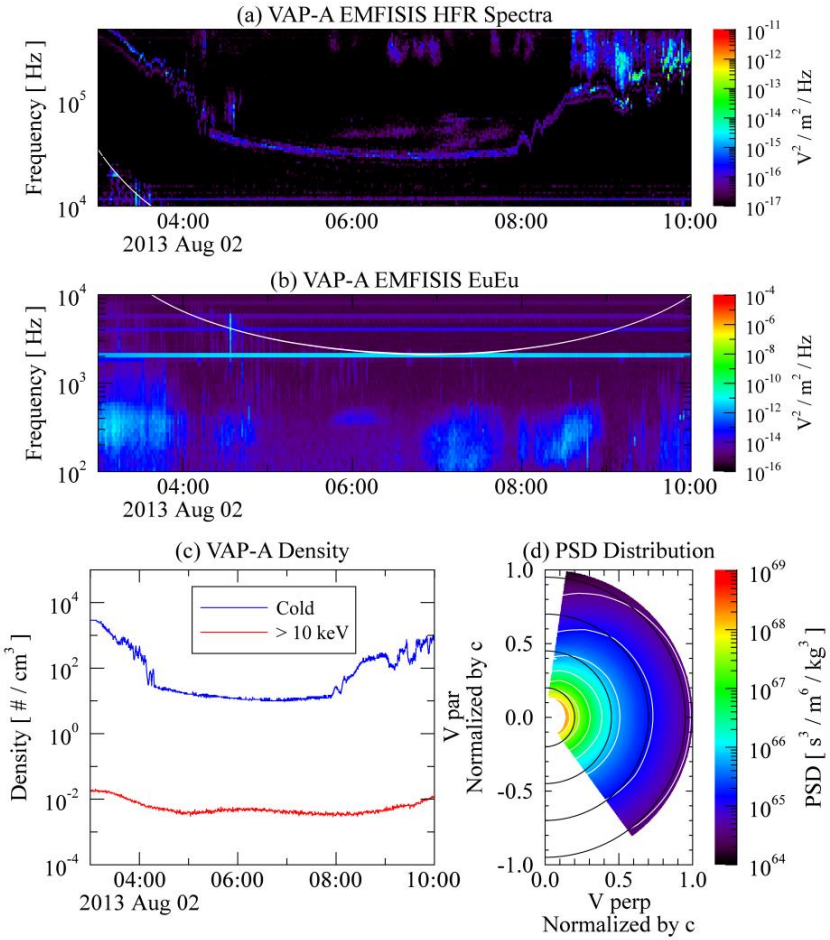

Figure 2. Plots of data taken on August 2, 2013. Panel (a) shows that a single upper hybrid band is manifested with no multiple harmonic cyclotron waves. Panel (b) shows the absence of whistler-mode chorus waves. Panel (c) indicates the densities for cold and hot electrons. Panel (d) shows the energetic electrons' PSD.

Case 3 :
Multiple harmonics UHR, chorus wave

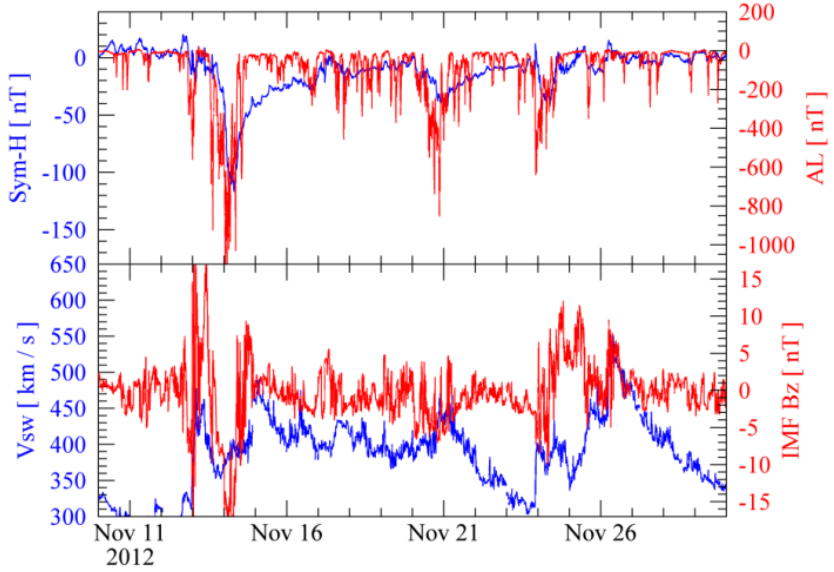

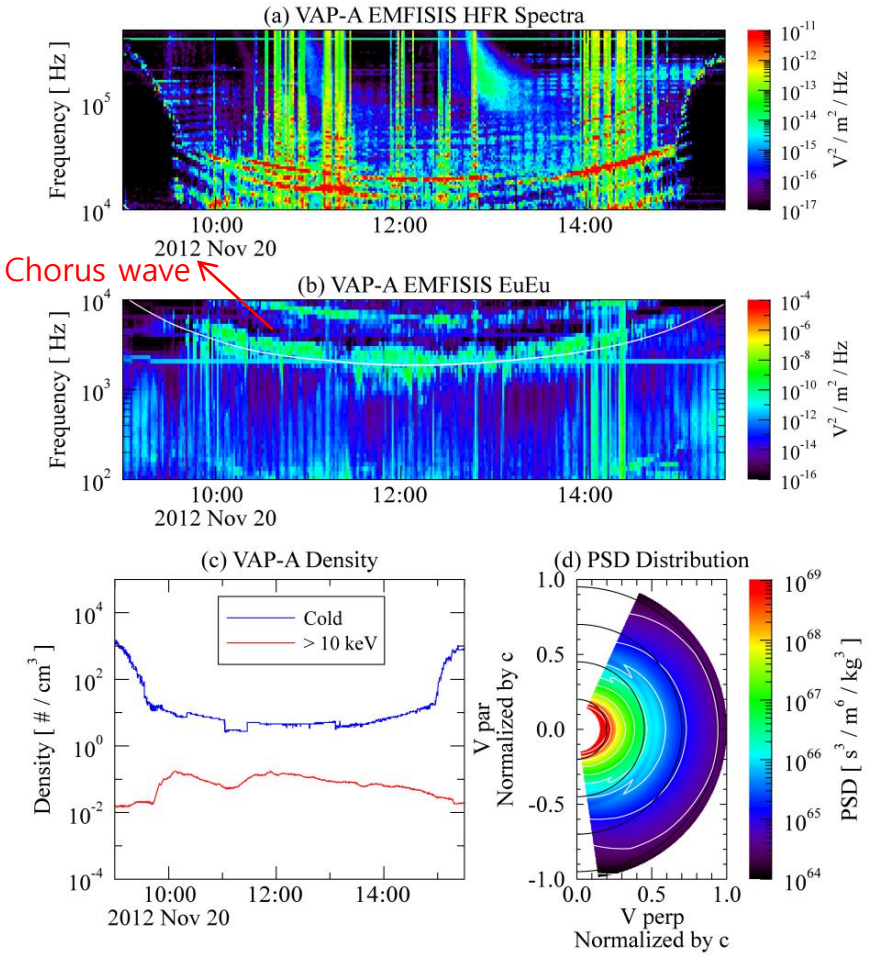

Figure 3. Data from November 20, 2012. Panel (a) displays the excitation of multiple harmonic electron-cyclotron waves above and below the upper hybrid frequency throughout the entire interval between 10:00 and 15:00. The white line indicates the upper hybrid frequency. Panel (b) displays the excitation of chorus waves. Panel (c) plots that the cold and hot electron densities. Panel (d) plots energetic electrons' PSD.

Comparison of energy spectra of three cases

Phase space density

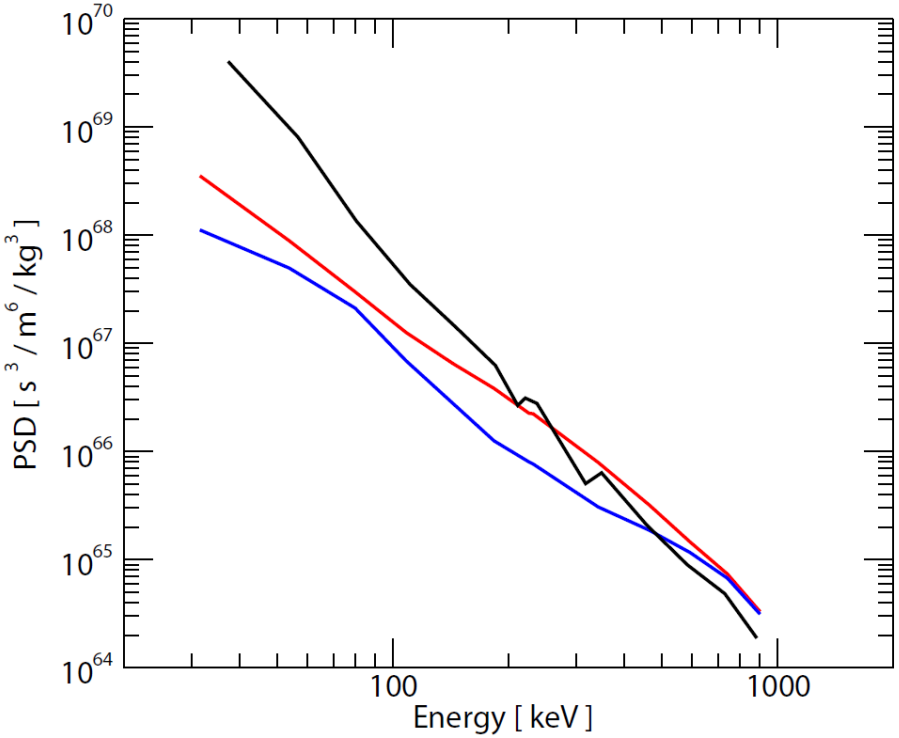

Red : case 1
Blue : case 2
Black : case 3

Generally case 1 shows more intensified energy spectrum than case 2.
Case 3 with chorus wave is higher in ~hundreds keV energy range, which coincides with substorm injected electrons' energy range.

Thermal Emission of Upper-Hybrid Fluctuations

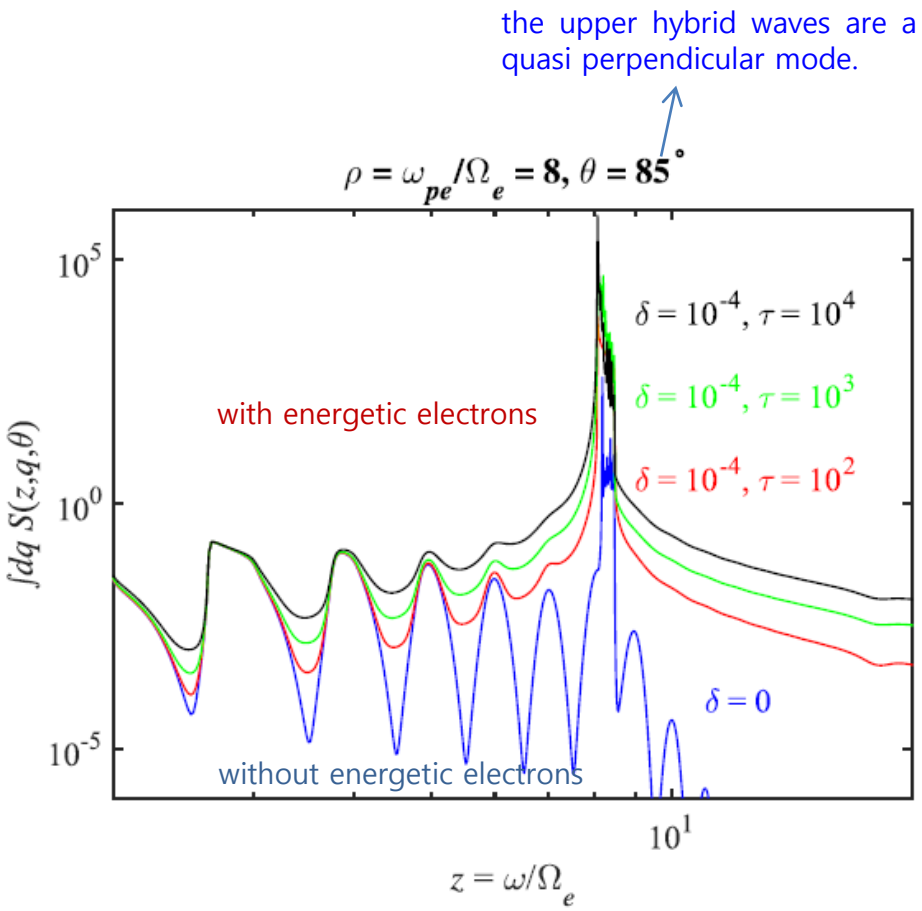

$$f_e(v) = \frac{n_c}{\pi^{3/2}\alpha_c^3}\exp\left(-\frac{v^2}{\alpha_c^2}\right) + \frac{n_h}{\pi^{3/2}\alpha_h^3}\exp\left(-\frac{v^2}{\alpha_h^2}\right),$$

$$\delta E^2_{\mathbf{k},\omega} = \sum_{a=c,h}\frac{T_a}{\pi^{5/2}\omega|\epsilon(\mathbf{k},\omega)|^2}\frac{n_a}{n_0}\frac{\omega_{pe}^2}{k^2\alpha_a^2}\sum_{n=-\infty}^{\infty}\xi_a I_n(\lambda_a)e^{-\lambda_a}\exp\left(-\zeta_n^{a2}\right),$$

$$\lambda_a = \frac{k_\perp^2\alpha_a^2}{2\Omega_e^2}, \qquad \xi_a = \frac{\omega}{k_\parallel\alpha_a}, \qquad \zeta_n^a = \frac{\omega - n\Omega_e}{k_\parallel\alpha_a},$$

$$\epsilon(\mathbf{k},\omega) = 1 + \sum_{a=c,h}\frac{n_a}{n_0}\frac{2\omega_{pe}^2}{k^2\alpha_a^2}\left[1 + \sum_{n=-\infty}^{\infty} I_n(\lambda_a)\,e^{-\lambda_a}\xi_a Z\left(\zeta_n^a\right)\right].$$

In terms of dimensionless quantities,

$$z = \frac{\omega}{\Omega_e}, \quad \rho = \frac{\omega_{pe}}{\Omega_e}, \quad \tau = \frac{T_h}{T_c}, \quad \delta = \frac{n_h}{n_0}, \quad q = \frac{k\alpha_c}{\Omega_e},$$
$$\lambda = \frac{q^2\sin^2\theta}{2}, \quad \Lambda_n(\lambda) = I_n(\lambda)e^{-\lambda}, \quad \xi = \frac{z}{q\cos\theta}, \quad \zeta_n = \frac{z-n}{q\cos\theta}, \qquad (6)$$

the normalized electric field intensity spectrum is given by

$$S(z,q,\theta) \equiv \frac{\pi^{5/2}\Omega_e\,\delta E^2_{\mathbf{k},\omega}}{T_h} = \frac{\rho^2 q^3\cos\theta}{\tau|\epsilon|^2}\sum_{n=-\infty}^{\infty}\left[(1-\delta)\Lambda_n(\lambda)\,e^{-\zeta_n^2} + \frac{\delta}{\tau^{1/2}}\Lambda_n(\tau\lambda)\exp\left(-\frac{\zeta_n^2}{\tau}\right)\right],$$
$$\epsilon = q\cos\theta\left[q^2 + 2\rho^2\left(1 - \delta + \frac{\delta}{\tau}\right)\right]$$

Figure 5. Spontaneously emitted electrostatic wave intensity with or without energetic electrons. The blue curve represents the case without energetic electrons, while the red curve depicts the case when tenuous energetic electrons are present. The highest intensity is associated with the upper hybrid frequency, multiple harmonic cyclotron modes below upper hybrid mode are also visible. Intensities for harmonic cyclotron modes are largely determined by the background electrons, as the blue and red curves almost coincide. For peak intensity at upper-hybrid frequency, the presence of 10^{-4} energetic electrons raises the maximum upper-hybrid intensity by an order of magnitude. For $\omega > \omega_{UH}$, the presence of energetic electrons leads to enhanced wave intensity.

Comparison between ES theory and observation

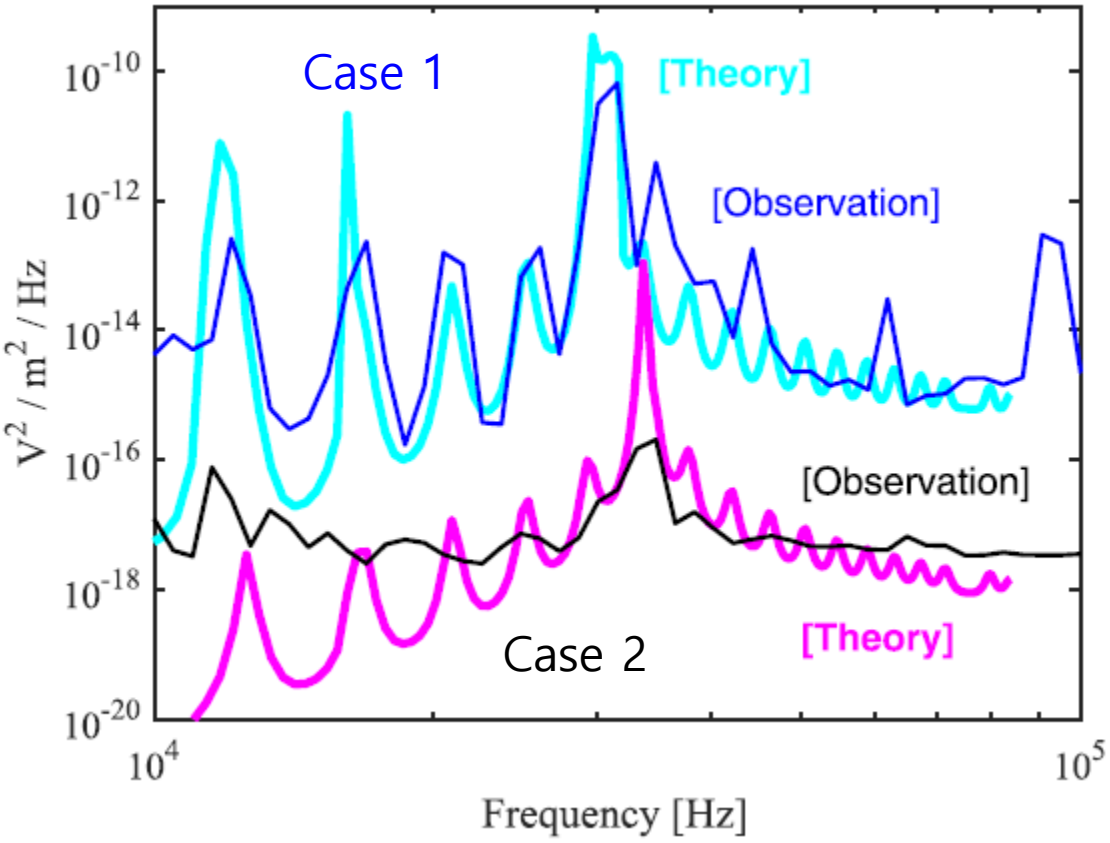

Figure 6. Wave power spectra shown in Figures 1 (May 8, 2013, 15:55 UT event); case 1 and Figure 2 (August 2, 2013, 05:30 UT); case 2 are plotted as a function of frequency, in blue and black, respectively. Theoretical results are superposed using cyan and magenta curves.

For May 8, 2013, 15:55 UT event, we chose $\rho = \omega_{pe}/\Omega_e \sim 7$ and $\delta = n_h/n_0 \sim 10^{-3}$, but since the temperature ratio $\tau = T_h/T_0$ is uncertain, we determined this ratio by trial and error. It turns out, the choice of $\tau = 10^2$ produced a reasonable fit. For the second case of August 2, 2013, 05:30 UT, we chose $\rho = 8$ and $\delta = 5 \times 10^{-5}$, and $\tau = 10^6$ is an appropriate choice.

Case 1 $$(\rho, \delta, \tau) = \left(\frac{\omega_{pe}}{\Omega_e}, \frac{n_h}{n_0}, \frac{T_h}{T_0}\right) = (7, 10^{-3}, 10^2).$$

Case 2 $$(\rho, \delta, \tau) = (8, 5 \times 10^{-5}, 10^6)$$

Spontaneously emitted **electromagnetic** upper hybrid and multiple harmonic electron cyclotron fluctuations

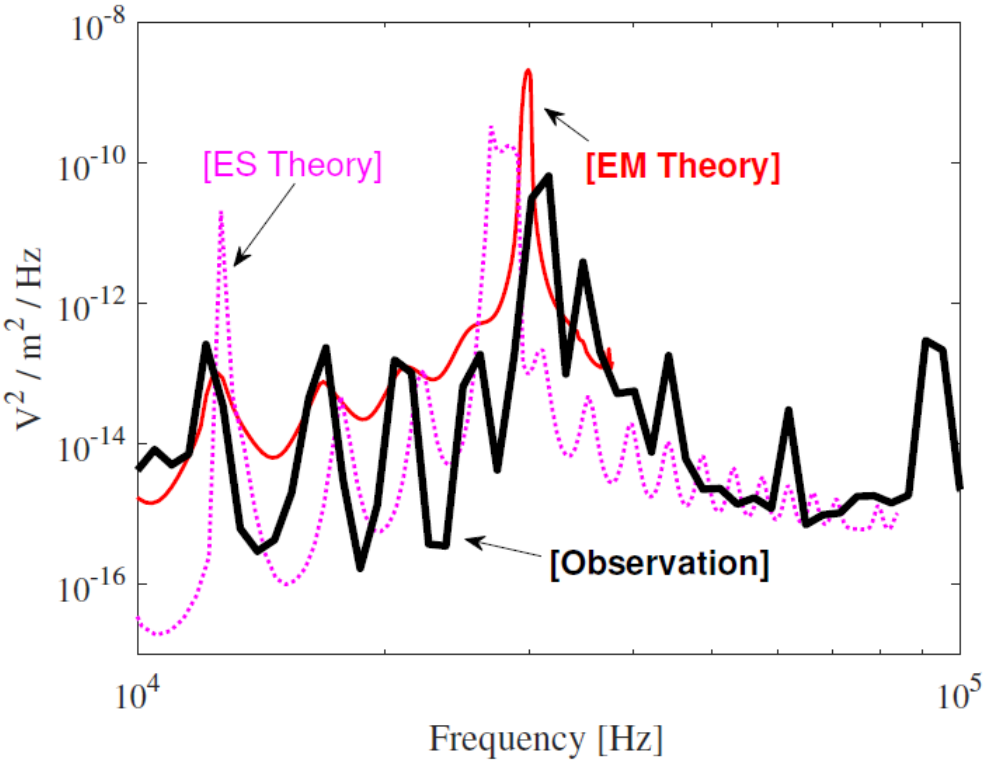

$$\langle \delta E^2 \rangle_{\mathbf{k},\omega} = \frac{1}{|\Lambda|^2}\Big[\left(|a_{11}|^2+|a_{12}|^2+|a_{13}|^2\right)K_{11}+\left(|a_{22}|^2+|a_{12}|^2+|a_{23}|^2\right)K_{22}$$
$$+\left(|a_{33}|^2+|a_{13}|^2+|a_{23}|^2\right)K_{33}-2\mathrm{Re}\left(a_{11}a_{12}^*+a_{22}a_{12}^*+a_{13}a_{23}^*\right)K_{12} \quad (1)$$
$$-2\mathrm{Re}\left(a_{11}a_{13}^*+a_{12}a_{23}^*+a_{33}a_{13}^*\right)K_{13}+2\mathrm{Re}\left(a_{12}a_{13}^*+a_{22}a_{23}^*+a_{23}a_{33}^*\right)K_{23}\Big],$$

and

$$\langle \delta B^2 \rangle_{\mathbf{k},\omega} = \frac{c^2k^2}{\omega^2|\Lambda|^2}\Big\{\frac{k_\parallel^2}{k^2}\Big[\left(|a_{11}|^2+|a_{12}|^2\right)K_{11}+\left(|a_{22}|^2+|a_{12}|^2\right)K_{22}$$
$$-\left(|a_{13}|^2+|a_{23}|^2\right)K_{33}+2\mathrm{Re}\left(a_{11}a_{12}^*+a_{12}a_{22}^*\right)K_{12}$$
$$-2\mathrm{Re}\left(a_{11}a_{13}^*+a_{12}a_{23}^*\right)K_{13}+2\mathrm{Re}\left(a_{22}a_{23}^*+a_{12}a_{13}^*\right)K_{23}\Big]$$
$$+\frac{k_\perp^2}{k^2}\Big[\left(|a_{12}|^2+|a_{13}|^2\right)K_{11}+\left(|a_{22}|^2+|a_{23}|^2\right)K_{22}$$
$$+\left(|a_{33}|^2+|a_{23}|^2\right)K_{33}-2\mathrm{Re}\left(a_{12}a_{22}^*+a_{13}a_{23}^*\right)K_{12}$$
$$-2\mathrm{Re}\left(a_{12}a_{23}^*-a_{13}a_{33}^*\right)K_{13}+2\mathrm{Re}\left(a_{22}a_{23}^*-a_{23}a_{33}^*\right)K_{23}\Big]$$
$$+\frac{2k_\perp k_\parallel}{k^2}\Big[\mathrm{Re}\left(a_{11}^*a_{13}\right)K_{11}+\mathrm{Re}\left(a_{12}^*a_{23}\right)K_{22}+\mathrm{Re}\left(a_{13}^*a_{33}\right)K_{33}$$
$$-\mathrm{Re}\left(a_{11}^*a_{23}+a_{12}^*a_{13}\right)K_{12}-\mathrm{Re}\left(a_{11}^*a_{33}+|a_{13}|^2\right)K_{13}$$
$$+\mathrm{Re}\left(a_{13}a_{23}^*+a_{12}a_{33}^*\right)K_{23}\Big]\Big\}, \quad (2)$$

Yoon, Hwang et al., GRL, submitted, 2018

Theoretical electric and magnetic field power spectra

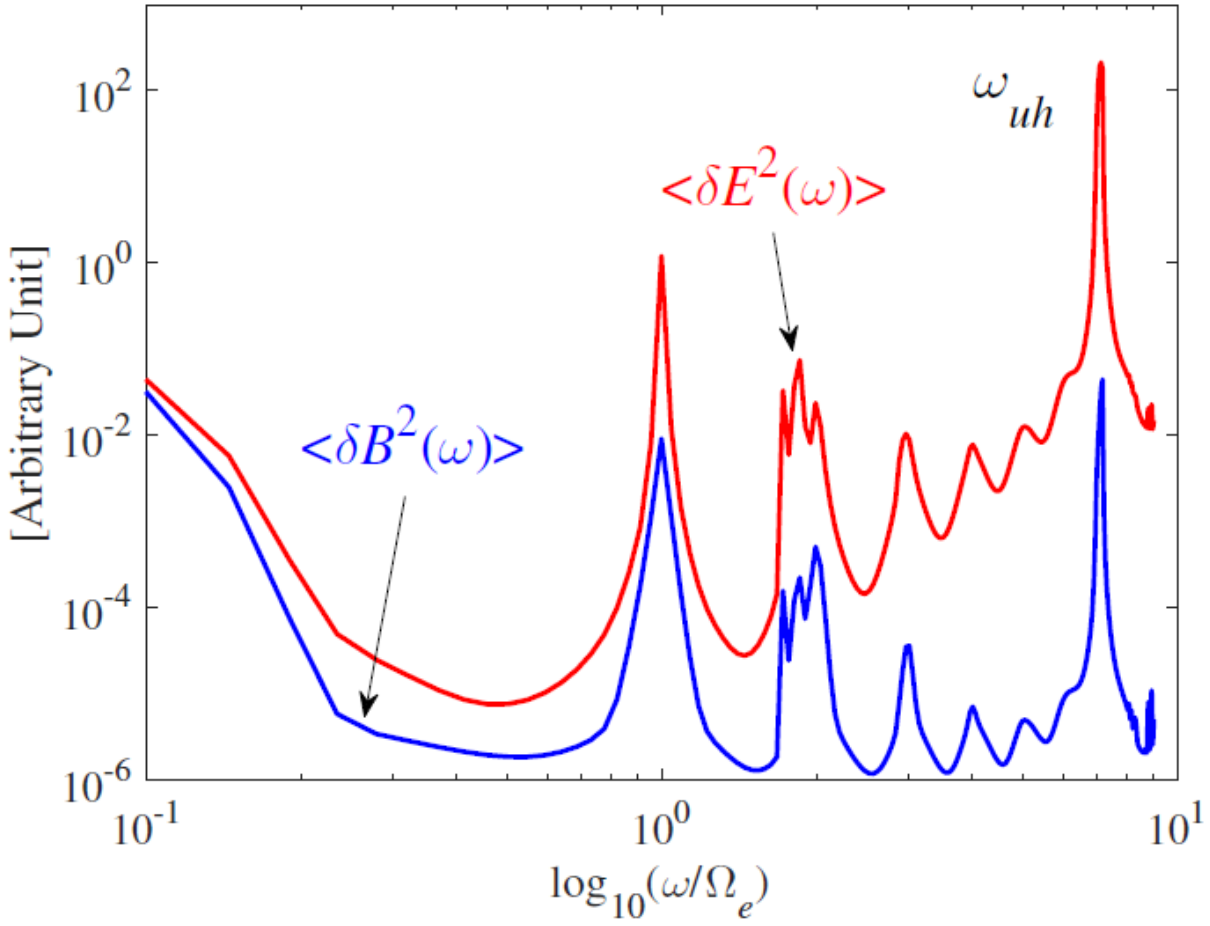

Yoon, Hwang et al., GRL, submitted, 2018

The Radio & Plasma Waves (RPW) instrument on Solar Orbiter

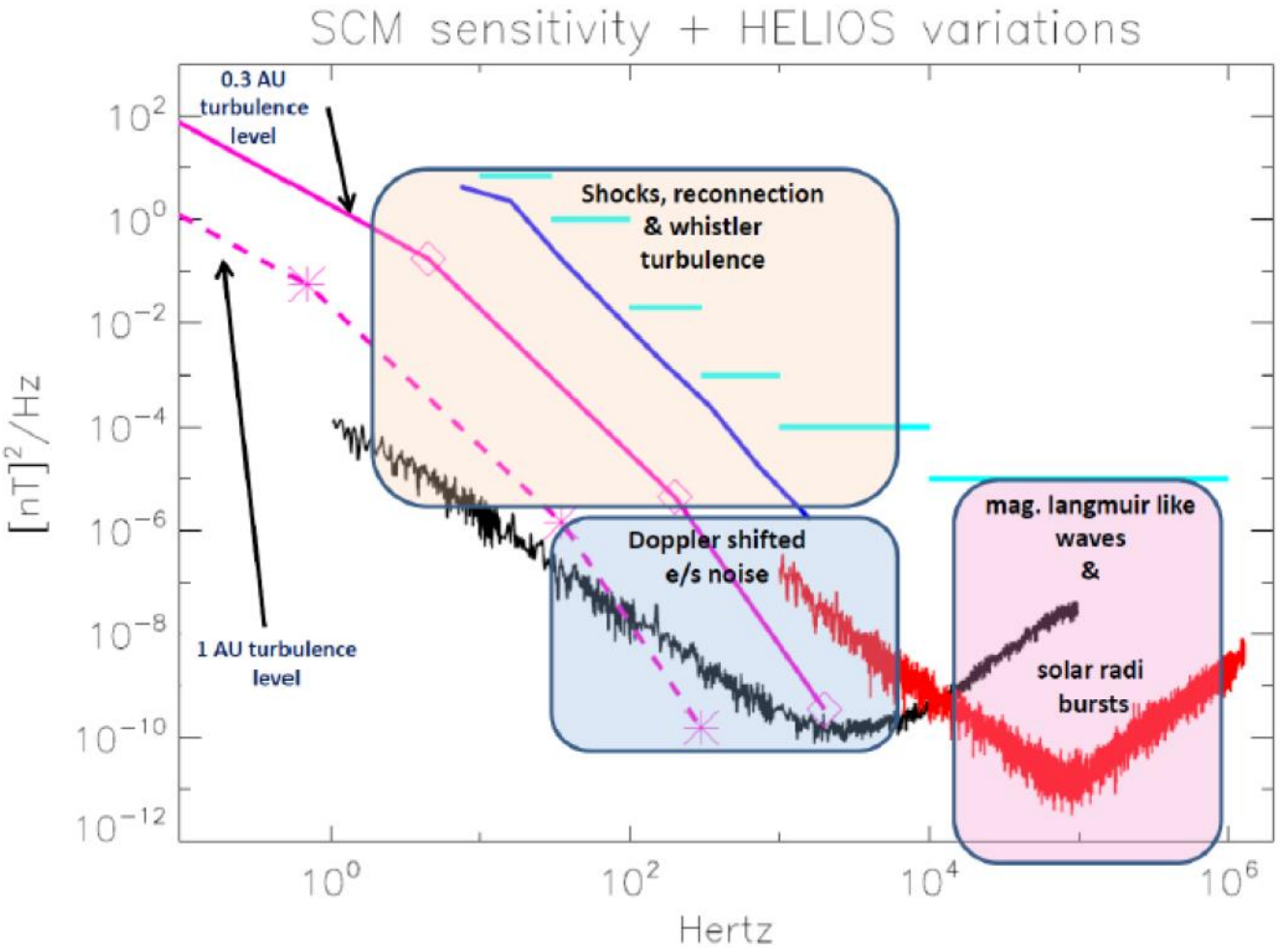

Figure 10: Magnetic field fluctuations of various natural phenomena that will be observed by the RPW instrument

Image Credit from Milan Maksimovic

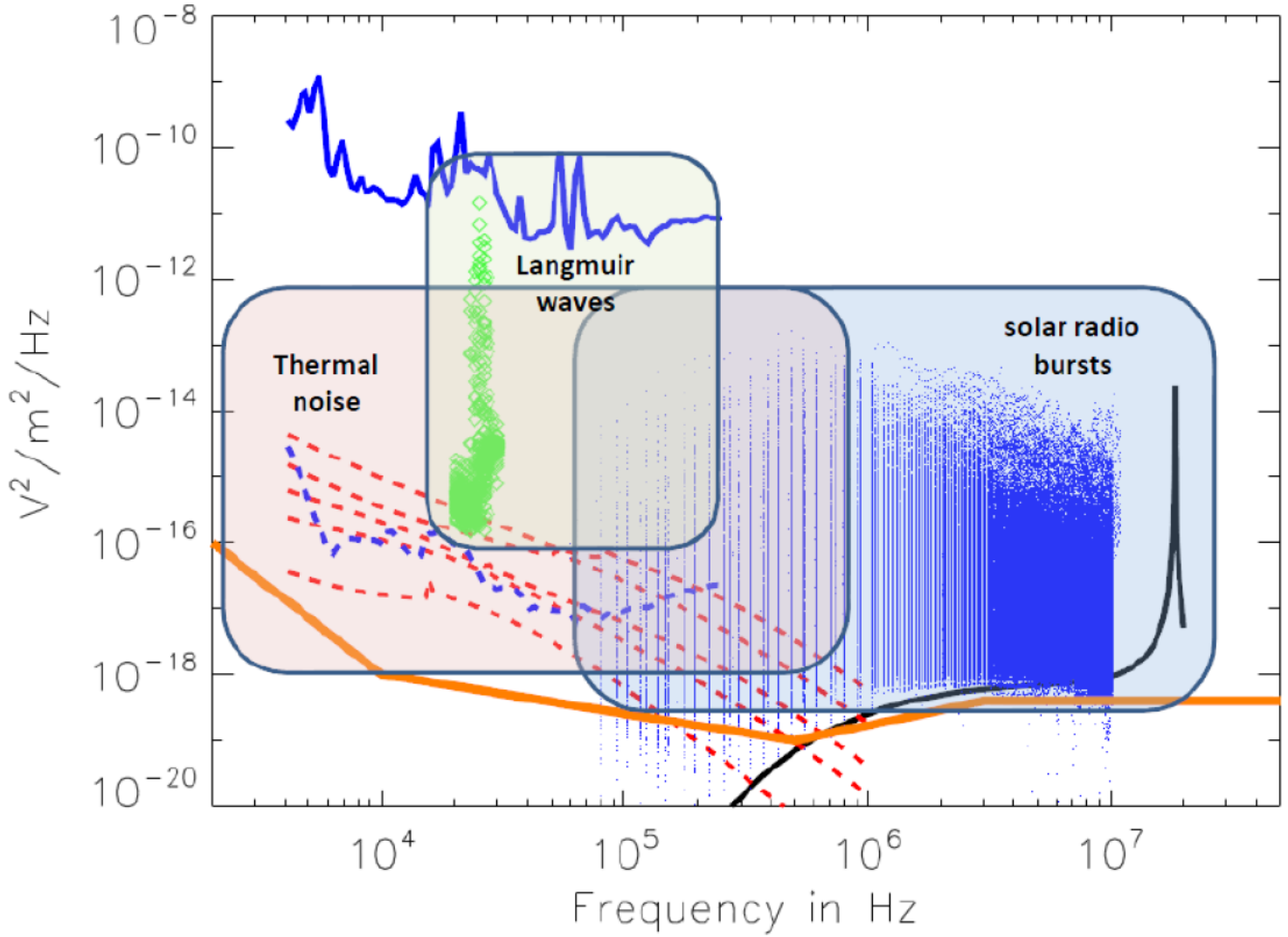

- RPW will measure both Langmuir waves and density fluctuations (from S/C pot. fluctuations, biased antennas) *DC E field and cross-shock potential.*
- RPW will measure simultaneously 2-axis E + 1 axis B up to 500 kHz → mode conversion

Summary

- Combined with ES theoretical calculation, it is demonstrated that the peak intensity associated with the upper-hybrid fluctuations is predominantly determined by energetic electrons in magnetized plasmas such as radiation belt.

- Denser and less background low energy electrons do not contribute much to the peak intensity but to the harmonics under upper hybrid frequency.

- This finding shows that upper-hybrid fluctuations detected during quiet time are useful not only for the determination of the low energy electron density, but also they contain information on the ambient energetic electron population as well.

- The electromagnetic effect is shown to be important for low-frequency ($f < f_{ce}$) regime, but even in the high-frequency regime, **there is a significant magnetic field component associated with the fluctuations.**

- **These results may not only be useful for interpreting existing spacecraft data but may also pose a potential new experimental goal for future spacecraft missions such as Parker Solar Probe and Solar Orbiter.**

EMIC Waves in Low Earth Orbit

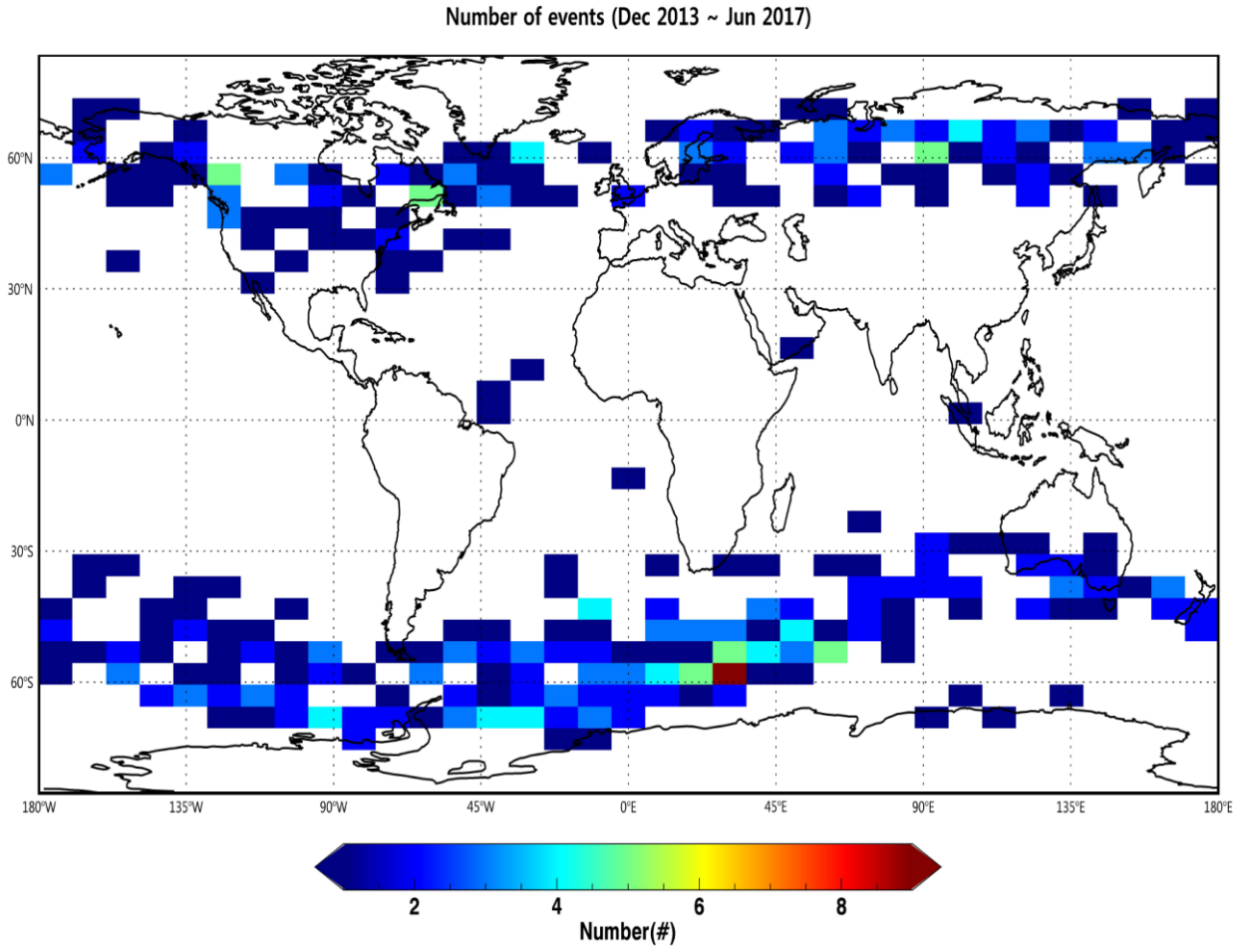

Swarm A, B and C

Inclination: ~88˚

Altitude: ~460-530km

velocity: 7.5km/s

Vector Field Magnetometer(VFM) resolution: 50 Hz

Kim et al., JGR 2018

Statistical properties of EMICs in LEO

			Duration threshold		
			1min	2min	3min
Total number of events #			433	170	77
Peak occurrence regions	MLAT		**45-65˚S , 45-60˚N**	40-65˚S , 40-55˚N	40-55˚S , 35-55˚N
	MLON		45˚W-45˚E	45˚W-45˚E	45˚W-45˚E
	MLT		**3-7**	3-6	2-7
Number of events depending on geomagnetic indices	Kp		**Peak occurrence at Kp < 4**	Peak occurrence at <4	Peak occurrence at <4
	Dst (for phases)	Initial phase	9 (2.1%)	5 (2.9%)	2 (2.6%)
		Main phase	11 (2.5%)	3 (1.8%)	1 (1.3%)
		Recovery phase 1	6 (1.4%)	4 (2.4%)	1 (1.3%)
		Recovery phase 2	**117 (27%)**	77 (45.3%)	35 (58.4%)
		No related	**290 (67%)**	81 (47.6%)	38 (36.4%)
Wave properties	Ellipticity		**Linear polarization**	Linear polarization	Linear polarization
	Normal angle		10-45˚	10-45˚	20-60˚
	Peak frequency		**0.4-1.6Hz**	0.4-1.6Hz	0.4-1.6Hz
	Peak amplitude		< 0.2 nT	< 0.2 nT	< 0.2 nT

Kim et al., JGR 2018

Conjunction event founder

Time evolution of propagating EMIC waves from space to the ground
by using multiple satellites and ground observations.

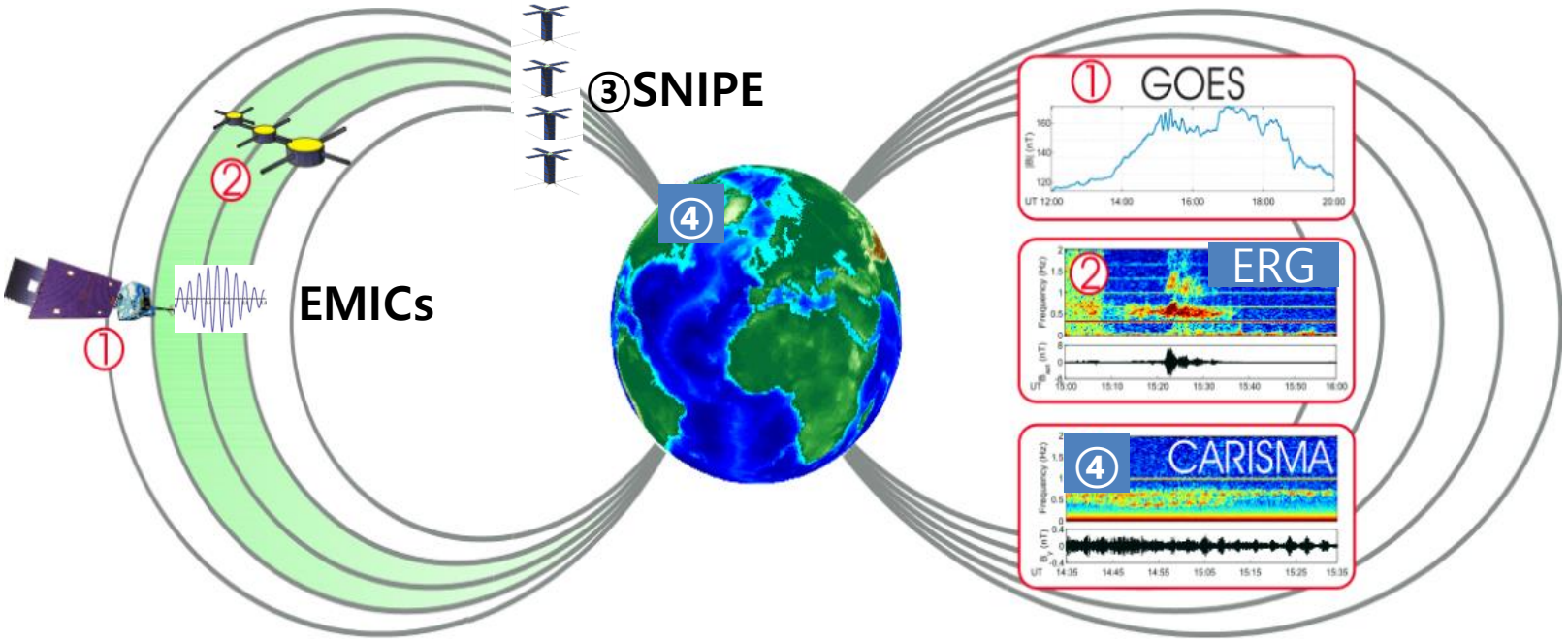

SNIPE mission (2017-2021)

- **New idea: Multi-satellite formation flying enables us to identify temporal and spatial variation**

- **How: KASI will launch SNIPE mission that consists of four nanosatellites in 2020.**

SNIPE (Small scale magNetospheric and Ionospheric Plasma Experiment)

- Constellation of four 6U-Nanosats (~10 kg for each satellite)
- Formation Flying (Slow separation from 10 km to 100 km for 6 months)
- Design life Time: 1 year (Science operation time: 6 months)
- Orbit: ~500 km – 600 km, Polar Orbit (Sun Synchronous Orbit)
- Launch in 2020

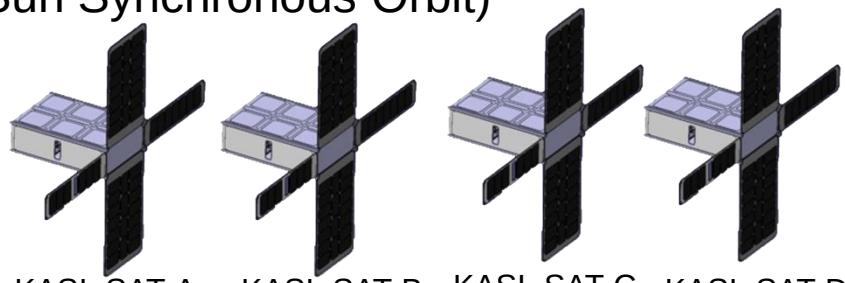

Timeline

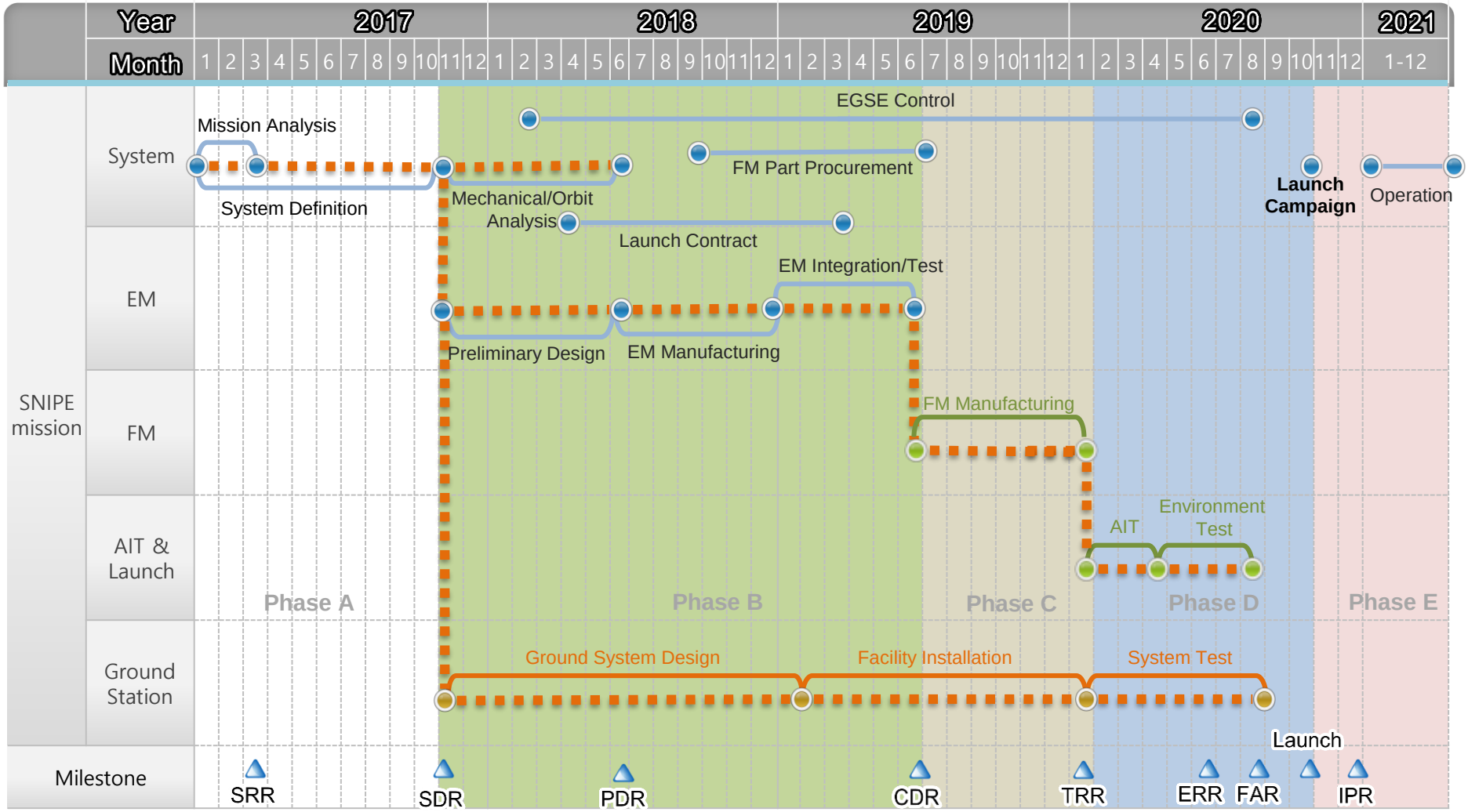
Year
2017
2018
2019
2020
2021
Month
1 2 3 4 5 6 7 8 9 10 11 12
1-12
SNIPE mission
System
EM
FM
AIT & Launch
Ground Station
Milestone
EGSE Control
Mission Analysis
System Definition
Mechanical/Orbit Analysis
FM Part Procurement
Launch Campaign
Operation
Launch Contract
EM Integration/Test
Preliminary Design
EM Manufacturing
FM Manufacturing
AIT
Environment Test
Phase A
Phase B
Phase C
Phase D
Phase E
Ground System Design
Facility Installation
System Test
Launch
SRR
SDR
PDR
CDR
TRR
ERR
FAR
IPR

Scientific Objectives

- **Science Targets**

✓ Spatial scale and energy dispersion of electron microbursts

✓ Temporal and spatial variations of plasma trough during magnetic storms

✓ Temporal and spatial variations of electron density and temperature in polar cap patches

✓ Measuring length of coherence for bubbles/blobs

✓ EMIC waves at the top of ionosphere

✓ Field aligned current in the ionosphere

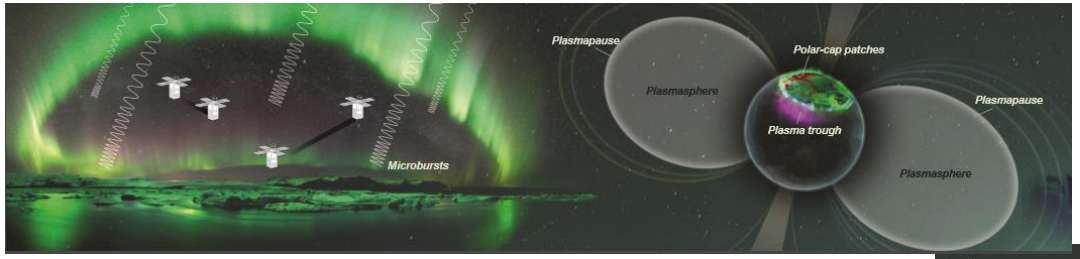

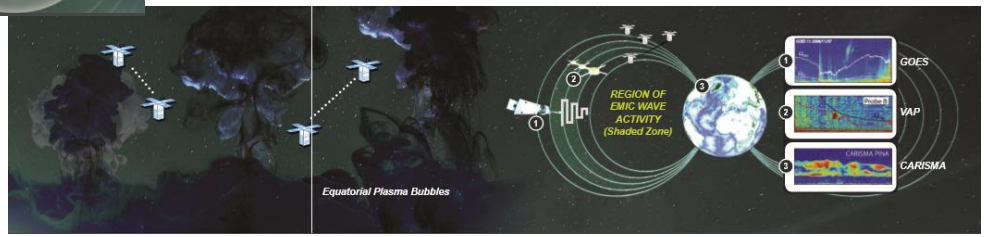

Spacecraft Platform

ADCS	Three-axis attitude control by reaction wheels Field align attitude control during microburst observation Accurate GPS system for position and velocity determination
CDHS	Time Sync between OBC and payloads Reliable communication between OBC and payloads with CAN BUS protocol
EPS	High efficiency solar cells High capacity Li-ion batteries
COMS	High speed S-band for science data downlink UHF command uplink Telemetry downlink: VHF
Propulsion	High performance micro-thruster

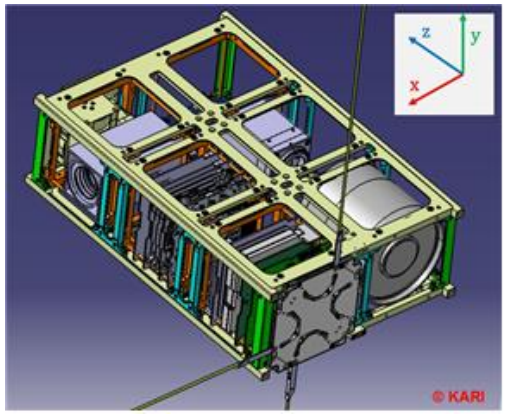

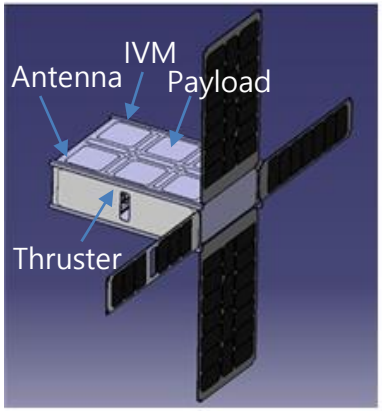

Formation Flying Strategy

Free Separation
(Commissioning
Phase)
~1 mon

Along track
formation
(Drift Recovery)
2-3 mon

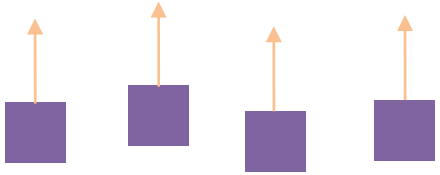

Cross track
formation
2-3 mon

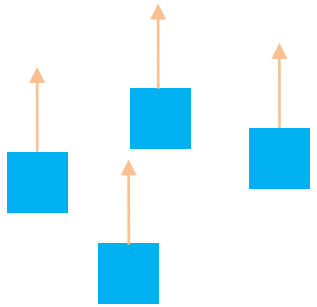

Non Control
(Extended)

Along Track Formation Flying

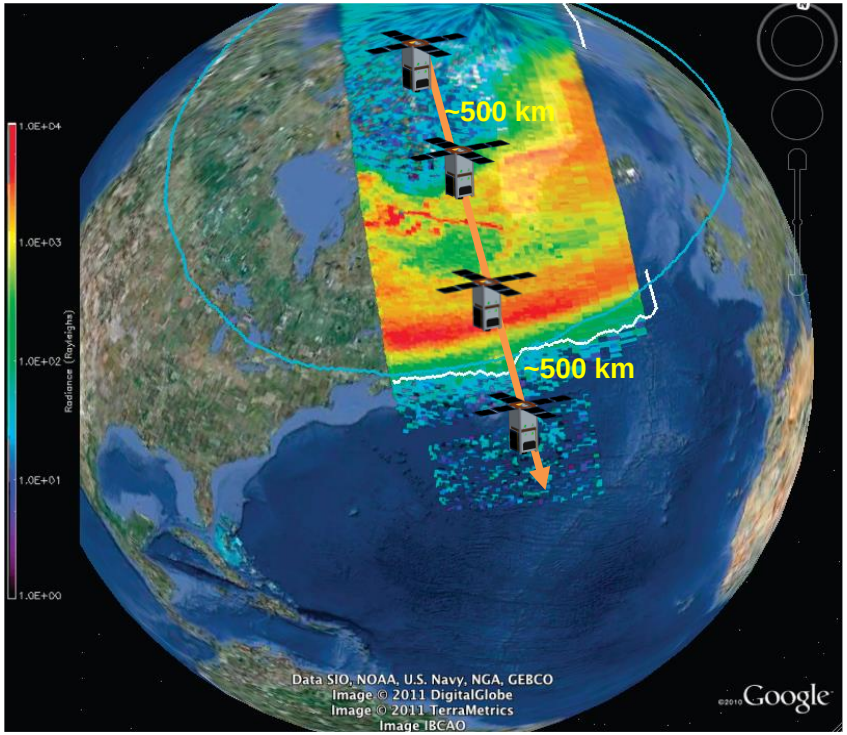

- After launch, each satellite distance shall increase automatically by initial speed difference.
- After commissioning phase, the spacecraft distance shall be controlled approximately 500 km.
- This formation enables to observe the temporal variation of small scale plasma structures.
- After along track observation, four spacecrafts shall get together in the box of 10 km x 10 km.

Polar Cap Patch Observation

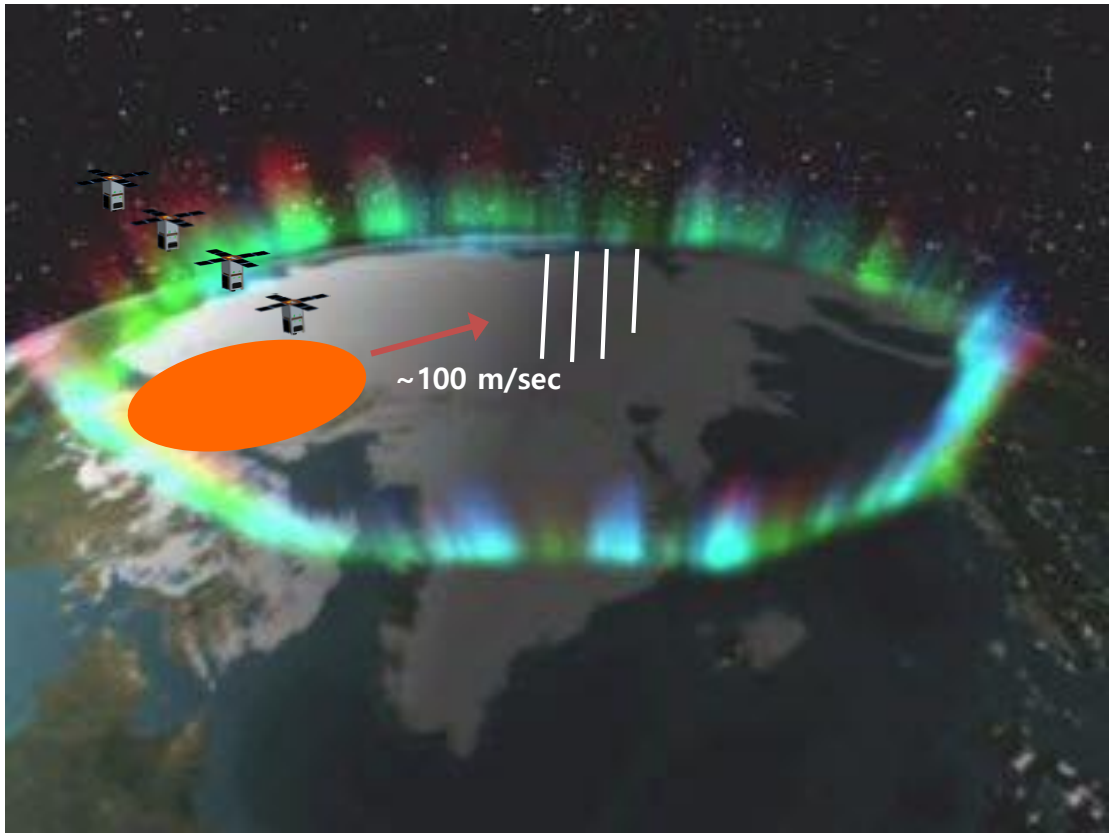

- Along track satellites pass through moving structures at different position.
- They shall provide two dimensional image of plasma patches

Science Operation

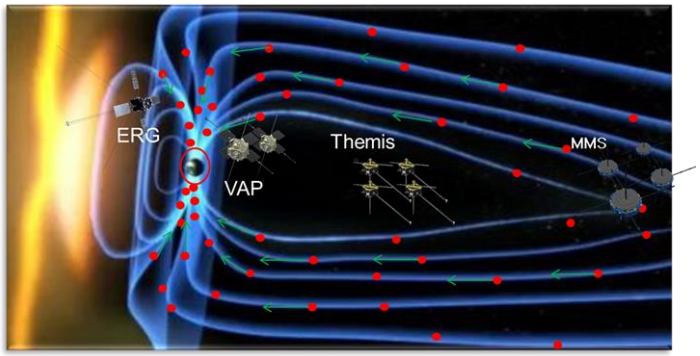

- Science operation at the conjugate points with large missions, Themis, MMS, VAP, Arase, GOES etc.
- Multipoint observation with other low earth orbit satellites like ICON, POES, DMSP, SWARM, many other Cubesats etc.
- Cooperation with ground observation like EISCAT, CARISMA etc.

Coronagraph on ISS (2017~2021)

Launch and Operation

- Diagnose temperature and velocity of the solar corona
- Understand the corona heating and solar wind acceleration
- FOV: 2.5 ~ 15 Rs
- Time cadence: 15 sec (Dynamic mode)
  90 min (Diagnostic mode)
- Launch to be installed on the ISS in 2021

Development Stages of ISS-COR

Total Solar Eclipse
(2017)

- Filters and Sensor
- EM(Engineering Model)

Balloon
(2018 - 2019)

- Occulter
- Electronic and Mechanical Parts
- QM (Qualification Model) Level
- Pointing System

ISS
(2020 - 2021)

- Complete Product
- FM (Flight Model)
- Pointing System

THANK YOU